Maintenance of α-Helical Structures by Phenyl Rings in the Active-Site Tyrosine Triad Contributes to Catalysis and Stability of Ketosteroid Isomerase from *Pseudomonas putida* Biotype B†

Gyu Hyun Nam,‡,⊥,§ Do Soo Jang,‡,⊥,§ Sun-Shin Cha,‡,∥ Tae-Hee Lee,‡,# Do-Hyung Kim,‡,$ Bee Hak Hong,‡,⊥ Young Sung Yun,‡,⊥ Byung-Ha Oh,‡,# and Kwan Yong Choi*,‡,⊥

Division of Molecular and Life Sciences National Research Laboratory of Protein Engineering, and National CRI Center for Biomolecular Recognition, Pohang University of Science and Technology, Pohang, 790-784, South Korea

Received May 29, 2001; Revised Manuscript Received September 10, 2001

ABSTRACT: Ketosteroid isomerase (KSI) from *Pseudomonas putida* biotype B is a homodimeric enzyme catalyzing an allylic rearrangement of Δ^5-3-ketosteroids at rates comparable with the diffusion-controlled limit. The tyrosine triad (Tyr14···Tyr55···Tyr30) forming a hydrogen-bond network in the apolar active site of KSI has been characterized in an effort to identify the roles of the phenyl rings in catalysis, stability, and unfolding of the enzyme. The replacement of Tyr14, a catalytic residue, with serine resulted in a 33-fold decrease of k_{cat}, while the replacements of Tyr30 and Tyr55 with serine decreased k_{cat} by 4- and 51-fold, respectively. The large decrease of k_{cat} for Y55S could be due to the structural perturbation of α-helix A3, which results in the reorientation of the active-site residues as judged by the crystal structure of Y55S determined at 2.2 Å resolution. Consistent with the analysis of the Y55S crystal structure, the far-UV circular dichroism spectra of Y14S, Y30S, and Y55S indicated that the elimination of the phenyl ring of the tyrosine reduced significantly the content of α-helices. Urea-induced equilibrium unfolding experiments revealed that the $\Delta G_U^{H_2O}$ values of Y14S, Y30S, and Y55S were significantly decreased by 11.9, 13.7, and 9.5 kcal/mol, respectively, as compared with that of the wild type. A characterization of the unfolding kinetics based on Φ_U-value analysis indicates that the interactions mediated by the tyrosine triad in the native state are very resistant to unfolding. Taken together, our results demonstrate that the internal packing by the phenyl rings in the active-site tyrosine triad contributes to the conformational stability and catalytic activity of KSI by maintaining the structural integrity of the α-helices.

Δ^5-3-ketosteroid isomerase (KSI)[1] is an enzyme catalyzing the allylic rearrangement of a variety of Δ^5-3-ketosteroids to Δ^4-3-ketosteroids by shifting a double bond from the 5(6)-position to the 4(5)-position (*1*). KSI is one of the most proficient enzymes enhancing the catalytic rate by a factor of 11 orders of magnitude as compared with the corresponding nonenzymatic reaction (*2*). Two KSIs from different bacterial species, *Pseudomonas putida* and *Comamonas testosteroni*, have been intensively studied as a prototype to understand the catalytic mechanism of the allylic rearrangement (*3*−*6*). These homologous KSIs share only 34% sequence identity, but the active-site residues are highly conserved (*7*, *8*).

Structural analysis by X-ray crystallography and NMR spectroscopy characterized the active-site geometry for efficient catalysis (*7*−*10*). Tyr14 and Asp99 (the residues of the *P. putida* KSI are numbered according to those of the *C. testosteroni* KSI throughout the text), which play crucial roles in catalysis, was found to form a direct hydrogen bond with the C3−O of the reaction intermediate analogue, d-equilenin, indicating that they contribute to the stabilization of the dienolate intermediate during catalysis (*7*, *11*). One of the most noticeable features of the active-site geometry is that the two catalytic residues Tyr14 and Asp99 are connected to Tyr30, Tyr55, and a water molecule forming a hydrogen bond network (Asp99···Wat504···Tyr14···Tyr55···Tyr30) at the bottom of the deep hydrophobic active-site cavity (*7*). The elimination of the hydroxyl group of Tyr14 or Tyr55 resulted in a decrease of $\Delta G_U^{H_2O}$ by 3.5−4.4 kcal/mol, suggesting that the H-bonded network mediated by Tyr14 or Tyr55 is important for the conformational stability (*12*). The double mutation, Y55F/D99L or Y30F/D99L, gave a synergistic effect on k_{cat} relative to their respective single mutations, suggesting that the H-bonded network provides the structural support for the enzyme to maintain the active-

† This research was supported by grants from the program of National Research Laboratory sponsored by Korean Ministry of Science and Technology, from Korea Science and Engineering Foundation, and in part by the Brain Korea 21 project.

* To whom correspondence should be addressed. Tel: 82-54-279-2295. Fax: 82-54-279-2199. E-mail: kchoi@postech.ac.kr.

‡ Division of Molecular and Life Sciences.

⊥ National Research Laboratory of Protein Engineering.

National CRI Center for Biomolecular Recognition.

§ These two authors contributed equally to this work.

∥ Current address: Beamline Research Division, Pohang Accelerator Laboratory.

$ Current address: Whitehead Institute for Biomedical Research, Nine Cambridge, Cambridge, MA 02142, USA.

[1] Abbreviations: KSI, ketosteroid isomerase; PLA_2, phospholipase A_2; $\Delta G_U^{H_2O}$, Gibbs free-energy change for unfolding in the absence of urea at 25 °C; Φ_U, ratio of the free-energy change determined from the kinetic data to that determined from urea equilibrium unfolding; SDS−PAGE, sodium dodecyl sulfate−polyacrylamide gel electrophoresis; pSK(−), pBluescript SK(−); EDTA, ethylenediaminetetraacetic acid; DTT, dithiothreitol; 5-AND, 5-androstene-3, 17-dione; CD, circular dichroism; UV, ultraviolet; H-bonded network, hydrogen-bonded network; WT, wild type; *B* factor, average temperature factor.

10.1021/bi015547k CCC: $20.00
Published on Web 10/20/2001

site geometry for efficient catalysis as well as for stability (*12*).

It has been reported that about 60% of the aromatic side chains of proteins are involved in aromatic pairs and 80% of them form networks of three or more interacting aromatic residues (*13*). Many lines of evidences have suggested that aromatic residues contribute to the stability of proteins when they occupy the interior of proteins for hydrophobic interactions (*14*−*16*). In barnase, the aromatic interactions by the side chains of tyrosine and phenylalanine residues were found to contribute to the protein stability by 1.3 kcal/mol (*14*). The crystal structure of the Y52F/Y73F double mutant of phospholipase A_2 (PLA_2) showed that the increased hydrophobic interactions of the phenyl groups compensate for the disrupted hydrogen bonds of the tyrosine residues (*15*). Even if the aromatic interactions have been known to be important for catalysis (*17*) as well as stability, the roles of the phenyl rings in the aromatic residues have not been well investigated in the enzymatic system.

In this study, the structural and functional roles played by the phenyl rings of three tyrosine residues, Tyr14, Tyr30, and Tyr55, in the active site of *P. putida* KSI were investigated. Those tyrosine residues were replaced respectively with serine to eliminate the aromatic-ring moiety. The mutational effects on catalysis together with the crystal structure of Y55S[2] provided an insight into the structural and functional roles of the phenyl rings in maintaining the active-site geometry for efficient catalysis. The structural analysis of Y55S by X-ray crystallography and the far-UV CD spectroscopy exhibited consistently that the mutation affected significantly the α-helical structure. Urea-induced equilibrium unfolding analysis also indicated that the mutations significantly decrease the conformational stability. Φ_U-value analysis revealed that the interactions mediated by three tyrosine residues in the native state are almost intact in the transition state for unfolding. Our results demonstrate that the phenyl rings in the active-site tyrosine triad are important for the conformational stability and the catalytic activity by maintaining the α-helical structures at the active site of KSI.

EXPERIMENTAL PROCEDURES

Reagents and Experimental Methods. Ultrapure urea was purchased from Sigma. T4 DNA ligase and restriction enzymes were obtained from Roche Molecular Biochemicals. Oligonucleotides were obtained from Bioneer Inc., Korea. Radiochemicals for sequencing were purchased from Amersham Pharmacia Biotech. 5-Androstene-3,17-dione (5-AND) was purchased from Steraloid Inc. 5-AND exhibited a single spot on the thin layer chromatographic analysis, and its molecular weight was confirmed by mass spectrometry as described previously (*18*). All other chemicals were molecular biology grade and obtained from Sigma. The protein concentration was determined utilizing the difference extinction coefficient (2330 M^{-1} cm^{-1} per tyrosine residue) between tyrosinate and tyrosine at 295 nm as described previously (*19*). The accuracy of the protein concentration was confirmed by the quantitative analysis of the bands on SDS−PAGE by use of an imaging densitometer (Bio-Rad, GS-700) and a software program provided by the manufacturer (Molecular Analyst/PC).

Site-Directed Mutagenesis. Tyrosine residues at 14, 30, and 55 positions were replaced individually with serine to make Y14S, Y30S, and Y55S according to the method described previously (*20*). Single-stranded and uracil-containing template DNA complementary to the coding strand of the isomerase gene was obtained from pSW2 (*21*), a recombinant pBluescriptSK(−) [pSK(−)] plasmid containing the *P. putida* KSI gene, which had been introduced in *Escherichia coli* RZ1030 after infection with the helper phage M13K07 (Amersham Pharmacia Biotech). The oligonucleotides of 5′-C CTG ATG GCC CGT AGC ATC GAG CTG GT-3′ for Y14S; 5′-GAT ATC GAG GCG ATC GTG CAG ATG TTC GCC GAT GAC G-3′ for Y30S; and 5′-CAG ATT GCC GCG TTC TCT CGG CAG GGT TTG GGC-3′ for Y55S were used as a primer for the respective mutagenesis; the underlined nucleotides represent those changed for mutations. The entire genes of the mutant isomerases were sequenced to confirm the desired mutations. The mutated gene inserted into pSK(−) was digested with *Eco*RI and *Hin*dIII to isolate the inserted DNA fragment containing the entire isomerase gene and then subcloned into *Eco*RI and *Hin*dIII sites of pKK223-3 (Amersham Pharmacia Biotech) to construct the recombinant plasmid for expression.

Expression and Purification of KSI Proteins. Each mutant KSI gene was expressed respectively in *E. coli* BL21(DE3). The mutant enzymes of Y30S and Y55S were expressed as soluble forms and purified by the deoxycholate affinity chromatography and gel-filtration chromatography according to the procedure described previously (*22*). The Y14S protein was expressed as inclusion body. The inclusion body was solubilized by 8 M urea and then dialyzed against a refolding buffer containing 20 mM potassium phosphate, pH 7.0, 0.5 mM ethylenediaminetetraacetic acid (EDTA), and 1 mM dithiothreitol (DTT). The dialyzed protein was then applied onto the deoxycholate affinity resin. The bound fraction was concentrated and subjected to gel-filtration chromatography similarly as that of other mutant proteins. The purity of the protein was confirmed by the presence of a single band on an SDS−PAGE analysis.

Determination of Enzyme Activity. The catalytic activities of the wild-type and mutant enzymes were determined spectrophotometrically using 5-AND as a substrate according to the procedure described previously (*22*). All the activities were determined by use of a UV spectrophotometer (Cary 3E) at 25 °C in the assay buffer containing 34 mM potassium phosphate, pH 7.0, and 2.5 mM EDTA with the respective substrate concentration, 12, 35, 58, 82, and 116 μM. The reaction was monitored at 248 nm for about 20% completion, and the initial linear reaction velocities were determined for 5% conversion of the substrate. The kinetic parameters, k_{cat} and K_M, were obtained by analyzing the data using the Lineweaver−Burk reciprocal plot. Mean values (± standard deviations) from three independent determinations were obtained for the comparison of kinetic parameters.

Crystallization and Structure Determination of Y55S. The crystals of the mutant protein were grown from a solution containing 1.2 M ammonium acetate and 0.1 M sodium acetate at pH 4.6 by the method of hanging drop vapor diffusion at 22 °C as described previously (*8*). Diffraction data were obtained by a DIP2020 area detector with graphite-

[2] The atomic coordinate of Y55S has been deposited with the entry code of 1K41 at Brookhaven Protein Data Bank.

monochromated Cu Kα X-rays, which were generated by a rotating anode generator (MacScience M18XHF) operated at 90 mA and 50 kV at room temperature. Data reduction, merging, and scaling were carried out with the programs DENZO and SCALEPACK as described previously (*23*). The structure of the mutant protein was determined by the molecular replacement method utilizing the atomic coordinates of the wild-type KSI (Brookhaven Protein Data Bank, code 1OPY). The omit map was used to avoid the phase bias which might give a wrong information in the construction of Y55S crystal structure.

CD Spectroscopic Analyses. Circular dichroism (CD) spectroscopic analyses were performed with a spectropolarimeter (JASCO 715). A cuvette with a path length of 0.2 cm was used for all the CD spectral measurements. The temperature of the cuvette was adjusted by use of a Peltier type temperature controller (Jasco PTC-348WI). KSI at 15 μM was incubated in the buffer containing 20 mM potassium phosphate, pH 7.0, 1 mM EDTA, and 1 mM DTT. The CD spectra were obtained at 25 °C with the scan speed of 10 nm/min and the bandwidth of 2 nm. Scans were collected at 0.2 nm intervals with a response time of 0.25 s and accumulated three times. All the CD spectra were corrected by subtracting the spectrum of the buffer solution and smoothed utilizing a program provided by the manufacturer of the spectropolarimeter.

Equilibrium Unfolding. For the measurement of the molar ellipticity of KSI at different urea concentrations, the enzyme at 15 μM was incubated in the buffer containing 20 mM potassium phosphate, pH 7.0, 1 mM EDTA, 1 mM DTT with different urea concentrations from 0 to 8 M longer than 48 h. The ellipticity at 222 nm was recorded and analyzed at the respective urea concentration.

The changes in the optical properties of the protein were compared by normalizing each transition curve with the apparent fraction of the unfolded form, F_U:

$$F_U = (Y_N - Y)/(Y_N - Y_U) \quad (1)$$

where Y is the observed molar ellipticity at a given urea concentration, and Y_N and Y_U are the observed values for the native and unfolded forms, respectively, at the same denaturant concentration. A linear dependence of Y on the denaturant concentration was observed in the baseline regions of both native and unfolded isomerases. Linear extrapolations from these baselines were made to obtain estimates of Y_N and Y_U in the transition region.

The equilibrium constant (K_U) and free-energy change (ΔG_U) for denaturation were determined according to a two-state model of denaturation by using the following equations (*12*):

$$K_U = 2P_T[F_U{}^2/(1 - F_U)] \quad (2)$$

$$\Delta G_U = -RT \ln(K_U) = \Delta G_U{}^{H_2O} - m[\text{urea}] \quad (3)$$

where P_T is the total protein concentration, $\Delta G_U{}^{H_2O}$ is the free-energy change in the absence of urea, and m is a measure of the ΔG_U dependence on urea concentration. The data of a urea denaturation curve were fitted to eq 4 (*24*) by a nonlinear least-squares analysis utilizing a graphic program (Abelbeck Software, Kaleidagraph version 2.6).

$$Y = Y_N - (Y_N - Y_U)\exp[(m[\text{urea}] - \Delta G_U{}^{H_2O})/RT]\{\{1 + 8P_T/\exp[(m[\text{urea}] - \Delta G_U{}^{H_2O})/RT]\}^{1/2} - 1\}/4P_T \quad (4)$$

The difference in the free-energy change for unfolding, $\Delta\Delta G_U$, between the wild-type KSI and each mutant protein was obtained from the following equation:

$$\Delta\Delta G_U = \Delta G_U - \Delta G_U{}^m \quad (5)$$

where ΔG_U and $\Delta G_U{}^m$ are the free-energy changes for unfolding of the wild-type and mutant proteins, respectively.

Kinetic Analyses of Unfolding. Kinetic measurements during the unfolding process for the wild-type and mutant KSIs were performed by use of a spectrofluorometer (Shimadzu RF-5301) equipped with a thermostatically controlled cell holder. The protein was dissolved in the buffer containing 20 mM potassium phosphate, pH 7.0, 1 mM EDTA, and 1 mM DTT. Reactions were initiated by diluting the protein samples by 20-fold into the same buffer with various concentrations of urea at 25 °C. The dead time of mixing was about 10 s for manual mixing. The kinetics for unfolding was monitored by measuring the fluorescence intensity at 315 nm after excitation at 285 nm. The final protein concentration was 15 μM. The rate constants were obtained by fitting the data to the following equation:

$$F_t = F_\infty + \sum[F_i \exp(-k_i t)] \quad (6)$$

where F_t and F_∞ are the amplitude at time t and the final state, respectively, F_i is the amplitude of the kinetic phase, and k_i is the rate constant for unfolding. Data fitting was performed utilizing the Kaleidagraph program as described above.

The unfolding rate constants, k_U, obtained at different urea concentrations were then analyzed according to eq 7:

$$RT \ln k_U = RT \ln k_U{}^{H_2O} + m_U{}^{\ddagger}[\text{urea}] \quad (7)$$

where $k_U{}^{H_2O}$ and $m_U{}^{\ddagger}$ are the unfolding rate constant in the absence of urea and the dependence of the unfolding rate constant on urea concentration, respectively. Free energy of activation for the unfolding of the isomerase was obtained by use of the eq 8:

$$\Delta G_U{}^{\ddagger} = \Delta G_U{}^{H_2O\ddagger} - m_U{}^{\ddagger}[\text{urea}] \quad (8)$$

where $\Delta G_U{}^{H_2O\ddagger}$ is the free-energy change for the unfolding transition state in the absence of urea, and $m_U{}^{\ddagger}$ represents a measure of the $\Delta G_U{}^{\ddagger}$ dependence on urea concentration. $\Delta G_U{}^{\ddagger}$ was obtained from the relationship $\Delta G_U{}^{\ddagger} = RT\ln(k_B T/h) - \ln k_U$, where k_B, T, and h are the Boltzman constant, the experimental temperature, and the Plank constant, respectively.

Φ_U-Value Analysis. The changes in free energy of activation for unfolding, $\Delta\Delta G_U{}^{\ddagger}$ between the wild-type and mutant proteins were obtained from the following equation:

$$\Delta\Delta G_U{}^{\ddagger} = \Delta G_U{}^{\ddagger} - \Delta G_U{}^{\ddagger m} \quad (9)$$

where $\Delta G_U{}^{\ddagger}$ and $\Delta G_U{}^{\ddagger m}$ are the free-energy changes of activation for unfolding of the wild-type and mutant proteins, respectively. The Φ-value of unfolding, Φ_U, is the ratio of

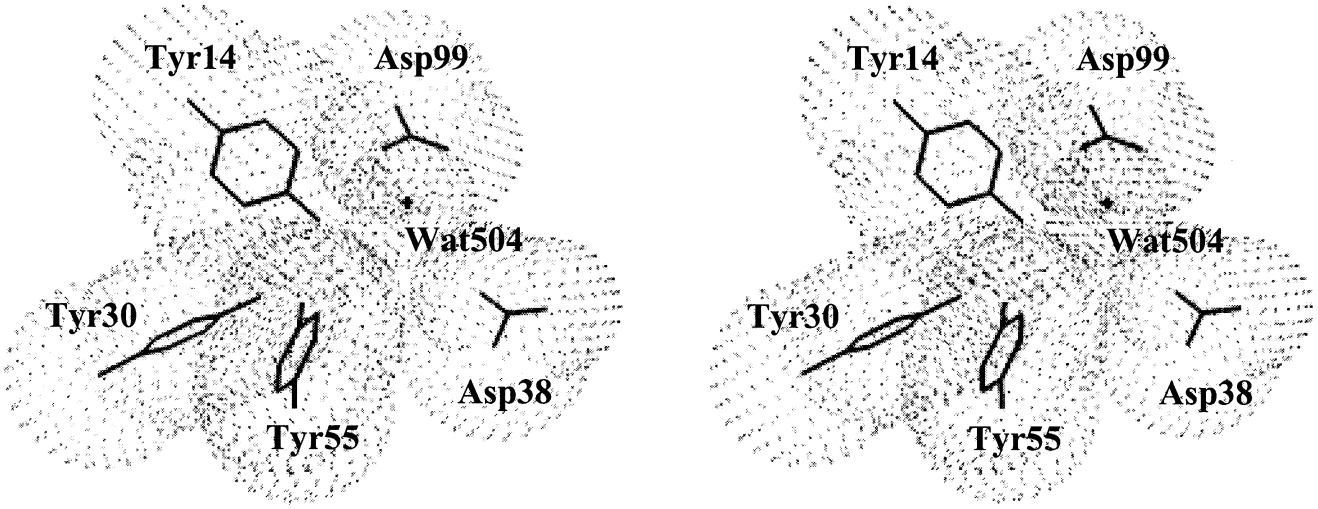

FIGURE 1: Stereoview of the active-site residues from *P. putida* KSI. The 150% van der Waals radius was drawn for each atom using the program Quanta, Version 2.0 (Molecular Simulations Inc.).

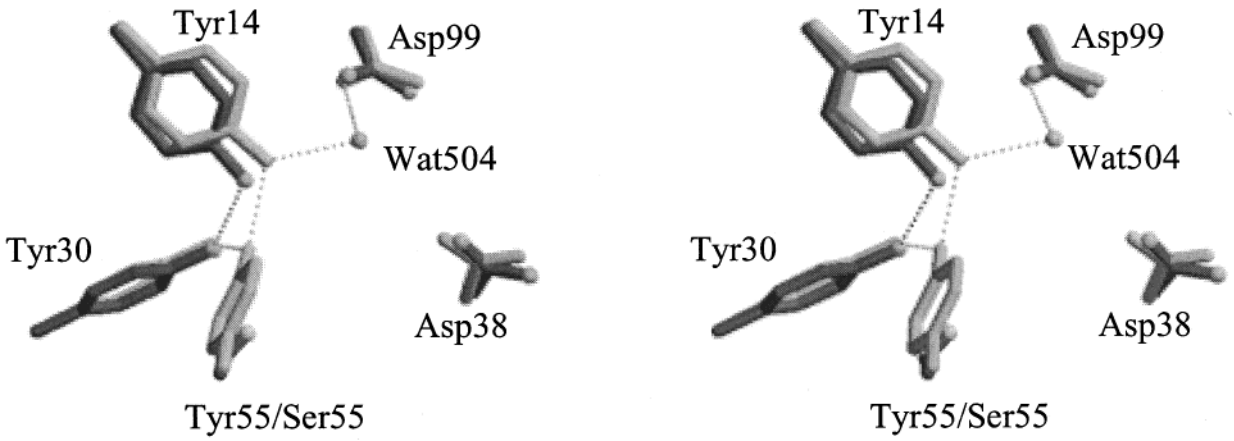

FIGURE 2: Stereoview of the active-site residues of WT and Y55S. WT (light gray) and Y55S (dark gray) are superimposed. The equivalent atoms of all the residues were used for the superposition of the structures. The putative hydrogen bonds are represented by dashed lines. Quanta version 2.0 (Molecular Simulation Inc.) was used for the superposition. Molscript (*31*) was used to draw the figure.

the free-energy change determined from the kinetic data to that determined from urea equilibrium unfolding experiment as the following equation:

$$\Phi_U = \Delta\Delta G_U^{\ddagger}/\Delta\Delta G_U = (\Delta G_F - \Delta G^{\ddagger})/(\Delta G_F - \Delta G_{solv}) \quad (10)$$

where ΔG_F is the difference of the noncovalent interaction energy between the wild-type and mutant enzymes in the folded states, $\Delta G^{\ddagger}$ is the difference in the transition states, and ΔG_{solv} is the difference in the unfolded states.

RESULTS

Structural Aspects of Three Tyrosine Residues. *P. putida* KSI contains four tyrosine residues at positions 14, 30, 55, and 115. On the basis of the atomic coordinates of the residues at the active site (*12*), Tyr14, 30, and 55 among these tyrosine residues were found to be close to one another forming a H-bonded network in the nonpolar active-site cavity (Figure 1). Tyr14 and Tyr55 are located on the α-helices A1 (Thr3−Val20), and A3 (Arg48−Leu59), respectively, while Tyr30 is located on the loop connecting α-helix A2 (Ile23−Met29) and *β*-strand B1 (Ala34−Pro39). Tyr14 makes a hydrogen bond with oxygen of a water molecule, Wat504, that forms a bridge between Tyr14 and Asp99 (Figure 2). The average temperature factor (*B* factor) of the hydroxyl group of Tyr14 is 14.1 (Table 1) and average *B* factor of the carbon atoms in the aromatic-ring moiety of Tyr14 is 6.3, suggesting that the phenyl group of Tyr14 is very rigid in motion. Consistent with this observation, the recent dynamic studies for *C. testosteroni* KSI free or complexed with D-equilenin, an intermediate analogue, revealed that motion of Tyr14 is significantly restricted (*25*−*27*). *B* factors of the carbon atoms in the aromatic-ring moiety and the hydroxyl group are 7.97 and 14.3 for Tyr30, and 12.6 and 18.5 for Tyr55, respectively (*12*). As reflected in these values, the hydroxyl groups are less rigid than the phenyl rings. Tyr14, Tyr30, and Tyr55 are completely buried within the protein interior except the OH group of Tyr14 and a small portion of the phenyl ring of Tyr55.

Mutational Effects on Catalysis. To analyze the mutational effects of Y14S, Y30S, and Y55S on the catalytic activity, the k_{cat} and K_M values of the mutant enzymes were determined using 5-AND as a substrate. The elimination of the phenyl ring from the respective tyrosine residue exhibited significant effect on k_{cat} rather than K_M. The Y14S mutation decreased k_{cat} by about 33-fold (Table 2). The mutational effect of Y14S was far less significant relative to that of

Table 1: Structural Features of Tyr Residues in the Wild-Type KSI

enzyme	secondary structure	SAA[a] of phenyl ring (Å^2)	SAA of OH group (Å^2)	*B* factor of Oη atom (Å^2)	*B* factor of aromatic ring moiety (Å^2)	H−Bond partner	H−bond distance[b] (Å)	*B* factor of the partner (Å^2)
Tyr14	helix	0	3	14.1	6.30	Tyr55 Oη	2.7 ± 0.32	18.5
						Wat504 O	2.8 ± 0.33	24.9
Tyr30	no	0	0	14.3	7.97	Tyr55 Oη	2.7 ± 0.32	18.5
Tyr55	helix	12	0	18.5	12.6	Tyr14 Oη	2.7 ± 0.32	14.1
						Tyr30 Oη	2.7 ± 0.32	14.3

[a] SAA represents the solvent-accessible area. [b] The length of a hydrogen bond between oxygen atoms. [c] Tyr30 is located on the loop connecting α-helix A2 and β-strand B1.

Table 2: Kinetic Parameters of KSI and Its Mutants[a]

enzyme	k_{cat} (s^{-1})	K_M (μM)	k_{cat}/K_M (M^{-1} s^{-1})	relative[b] k_{cat}	relative[c] K_M
WT[d]	21230 ± 810	49.9 ± 1.3	(4.3 ± 0.2) × 10^8	1.00	1.00
Y14S	644 ± 56	26.2 ± 3.1	(2.4 ± 0.4) × 10^7	0.03	0.53
Y30S	5410 ± 107	44.9 ± 2.8	(1.2 ± 0.1) × 10^8	0.25	0.90
Y55S	415 ± 34	64.0 ± 2.1	(6.5 ± 0.2) × 10^6	0.02	1.28

[a] The assays were performed in the buffer containing 34 mM potassium phosphate and 2.5 mM EDTA, pH 7.0. The kinetic parameters were determined from three independent measurements. [b,c] Values relative to those of WT. [d] Values from Kim et al. (*30*).

Table 3: Crystallographic Data and Refinement Statistics for Y55S

resolution (Å)	2.2
R_{sym}(%)	7.0
data completeness, $F > 1\sigma$(%)	94.9
$R_{standard}$ (%)	23.5
R_{free} (%)	31.9
no. of atoms	2296
water molecules	42
average *B* factor	27.209
rmsd bond length (Å)	0.083
rmsd bond angles (deg)	3.172
Ramachandran plot (%)	
most favored regions	81.9
additional allowed regions	16.7
disallowed regions	1

Y14F in which k_{cat} decreased by 2000-fold, indicating that the hydroxyl group of Ser14 plays a critical role in catalysis. The Y30S mutation marginally decreased k_{cat} by about 4-fold. Interestingly enough, the mutational effect of Y55S where k_{cat} was decreased by about 51-fold was more significant than that of Y14S, suggesting that the phenyl ring of Tyr55 might play a role more importantly than that of Try14.

Crystal Structure of Y55S. To understand the observed mutational effect on catalytic efficiency and maintenance of α-helix at the molecular level, the crystallization of the mutant enzymes was attempted, and only the crystals of Y55S could be obtained successfully. The crystal structure of Y55S was determined at 2.2 Å resolution with *R* value of 23.5%. It belongs to the space group *C*2 with cell dimensions $a = 88.889$ Å, $b = 73.135$ Å, $c = 51.156$ Å, and $\beta = 89.847$, which are almost the same as those of the crystal structure of the wild-type KSI complexed with D-equilenin, an intermediate analogue. The statistics of the crystallographic data and refinement are summarized in Table 3. Figure 3 shows the electron density maps for α-helix A3 in WT and Y55S, respectively. An omit map was used to define the reliable electron density of α-helix A3 in the Y55S structure (*28*). At an initial refinement stage, the structure was disturbed at 1000 K when the segment (residues 53−57) of α-helix A3 and the residues within 3.5 Å from the segment were omitted. The electron density map was calculated with the omission. α-Helix A3 displays poor electron densities for Y55S in an omit map (Figure 3B), suggesting that the secondary structure was significantly disrupted by the mutation. In addition, *B* factors of the atoms in α-helices, A1, A2, and A3 of Y55S, increased substantially as compared with those of WT (Figure 4), indicating that α-helices, A1, A2, and A3 were highly flexible even though electron densities of A1 and A2 were well defined in the mutant. From the structural comparison between WT and Y55S, the elimination of the aromatic moiety from a tyrosine yielded not only the structural changes of the active site in the mutant enzyme (Figure 2) but also the loss of the structural integrity for α-helix on which Tyr55 is located (Figure 3). The Y55S mutation led to the positional displacement of the phenolic moiety of Tyr14 toward Tyr30 (Figure 2). The distance between Tyr14 Oη and Tyr30 Oη became closer up to 3.0 ± 0.32 Å with a standard deviation on the basis of the estimation by Luzzati plots (*29*). This movement seems to affect the H-bonded network of the tyrosine triad. Wat504 mediating the H-bonded network, Tyr14···Wat504···Asp99, in the wild-type and Y55F structures (*30*) was not found in the Y55S structure. Thus, the Y55S mutation gave rise to the disruption of the H-bonded network, while the distance between Tyr14 Oη and Asp99 Oδ2 was increased by 0.6 ± 0.33 Å.

CD Spectra of Mutant Enzymes. The previous study showed that the respective replacement of three tyrosine residues, Tyr14, Tyr30, and Tyr55, with phenylalanine did not change significantly the overall conformation of the protein (*12*). When the structural changes of the three mutant enzymes with tyrosine-to-serine replacement were investigated by CD spectroscopy, the far-UV CD spectra of the mutant enzymes indicate modest but significant conformational changes in all three mutants (Figure 5). The molar ellipticity at 222 nm was decreased by about 3800, 5200, and 3400 deg cm^2 dmol^{-1} for Y14S, Y30S, and Y55S, respectively, as compared with that for WT, suggesting that the mutations perturb the α-helices leading to the structural change due to a decrease in the helical contents of the mutant enzymes as compared with that of WT. With the crystal structure of Y55S, these results suggests that the decrease of activity seems to be correlated with loss of ellipticity due to the structural alterations in the active site.

Mutational Effects on Conformational Stability. The equilibrium unfolding experiment was carried out by monitoring the molar ellipticity of the respective protein at 222 nm (Figure 6). The transition curve was normalized by assuming that the ellipticity at 222 nm for the native and unfolded states can be extrapolated linearly into the transition zone.

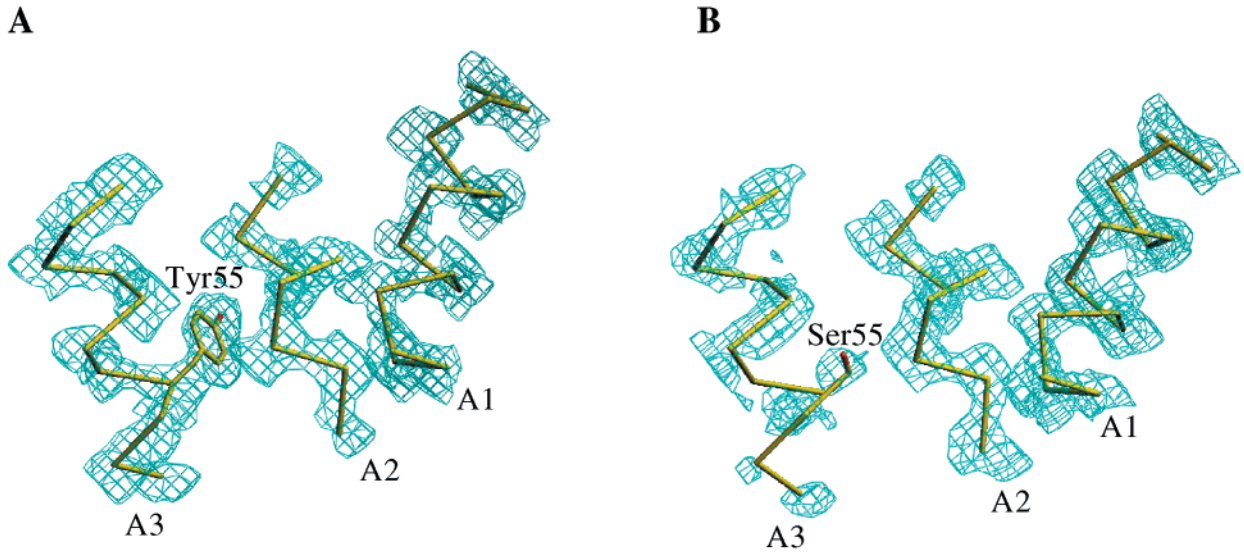

FIGURE 3: $2F_o - F_c$ electron density maps of the α-helices, A1 (Thr3−Val20), A2 (Ile23−Met29), A3 (Arg48−Leu59), surrounding Tyr55 for WT (A) and Ser55 for Y55S (B). For the electron density map of Y55S contoured at 1.0 σ, a simulated annealing $2F_o - F_c$ omit map was calculated and used to avoid the phase bias. The structures were displayed using the graphic software O (*31*). The original α-helical backbones of the wild-type KSI are traced as heavy lines to compare with the mutant KSI structure whose α-helical structure, A3, is significantly disrupted.

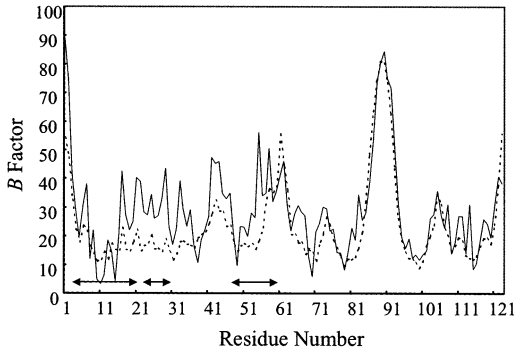

FIGURE 4: *B* factors of the main chain atoms in the structures of WT (broken line) and Y55S (solid line). Indicated arrows represent the respective α-helices, A1 (Thr3−Val20), A2 (Ile23−Met29), A3 (Arg48−Leu59), respectively.

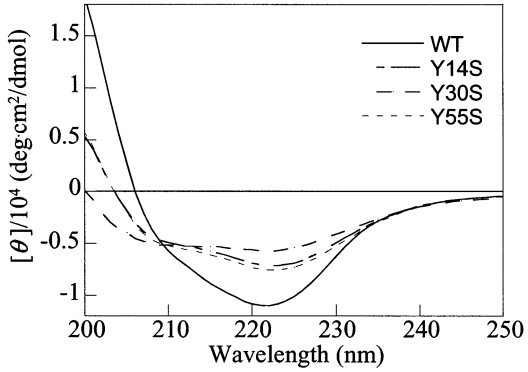

FIGURE 5: Circular dichroism (CD) spectra of WT, Y14S, Y30S, and Y55S in the far UV region (200−250 nm). Experiments were performed with the isomerase (15 μM) in the buffer containing 20 mM potassium phosphate, pH 7.0, 1 mM EDTA, and 1 mM DTT. The temperature was 25 °C and the cell path length was 0.2 cm.

There was no indication of any folding intermediates in the unfolding transition curve. The transition curves were almost coincident within experimental error for CD measurements. These results strongly suggest that KSI folding can be described as a two-state model without any folded intermediate at equilibrium. By applying a two-state model, the values of $\Delta G_U^{H_2O}$, m, $[\text{urea}]_{50\%}$, and $\Delta\Delta G_U$ for the wild-type and mutant enzymes were obtained (Table 4). The Y14S mutation decreased $\Delta G_U^{H_2O}$ by about 11.9 kcal/mol, and the midpoint of the unfolding transition curve, $[\text{urea}]_{50\%}$, was lowered to 2.00 M. The decrease of stability of Y14S is significant in contrast with that of Y14F, for which $\Delta G_U^{H_2O}$ was decreased by about 4.4 kcal/mol and the midpoint was shifted to 2.3 M (*12*), suggesting strongly that the phenyl ring of Tyr14 is important for the stability of KSI. The elimination of the phenyl ring from Tyr30 also destabilized the protein by about 13.7 kcal/mol. Since the conformational stability was affected little upon the Y30F mutation (*12*), the large decrease in structural stability can be attributed to the important role of the aromatic moiety of Tyr30. The Y55S mutation resulted in a decrease of stability by about 9.5 kcal/mol, which is about 6.0 kcal/mol bigger as compared with Y55F. All these results suggest that the phenyl rings of the tyrosine triad

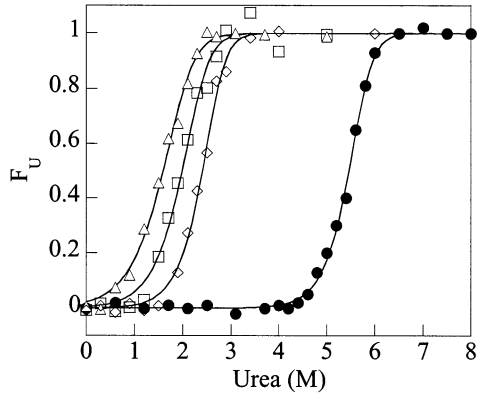

FIGURE 6: Unfolding equilibrium transition curves of WT (●), Y14S (□), Y30S (△), and Y55S (◇). The fraction of unfolded protein at each urea concentration was calculated from the molar ellipticity at 222 nm after correction for the pre- and post-transition baselines. The data were obtained with 15 μM of each protein in the buffer containing 20 mM potassium phosphate, pH 7.0, 1 mM EDTA, and 1 mM DTT. The data points were fitted to the eq 4 to obtain the transition curve.

Table 4: Changes in the Free Energies of Unfolding of Wild-Type and Mutant KSIs in the Reversible Denaturation with Urea[a]

enzyme	$\Delta G_U^{H_2O}$ (kcal/mol)[b]	m[c] (kcal/mol·M)	$[urea]_{50\%}$[d] (M)	$\Delta\Delta G_U$[e] (kcal/mol)
WT	24.3 ± 0.5	3.39 ± 0.07	5.22 ± 0.10	
Y14S	12.4 ± 0.3	2.93 ± 0.02	1.99 ± 0.07	11.9
Y30S	10.6 ± 0.4	2.55 ± 0.03	1.56 ± 0.09	13.7
Y55S	14.8 ± 0.4	3.43 ± 0.04	2.41 ± 0.09	9.5

[a] Measurements were performed at 25 °C and pH 7.0. Values were obtained by fitting the data from Figure 6 to the eq 4. [b] $\Delta G_U^{H_2O}$ was determined by extrapolation of the data to 0 M urea concentration during denaturation. [c] m is the slope of the linear denaturation plot, $d\Delta G_U/d[urea]$. [d] $[urea]_{50\%}$ is the concentration of urea at which 50% of the protein is unfolded. [e] Values obtained from the eq 5.

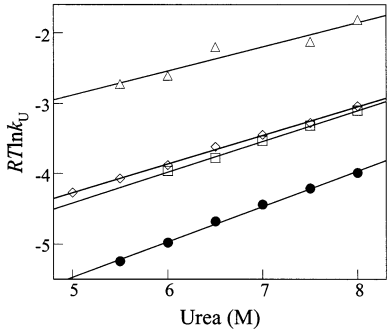

FIGURE 7: Plots of log k_U versus [urea] for WT (●), Y14S (□), Y30S (△), and Y55S (◇). Rate constants were measured in units of min^{-1}. All experiments were performed in the buffer containing 20 mM potassium phosphate, pH 7.0, 1 mM EDTA, and 1 mM DTT. The unfolding process was monitored by measuring the change in the intrinsic fluorescence intensity of the protein (excitation wavelength = 285 nm, emission wavelength = 325 nm).

contribute to conformational stability of KSI more significantly than the hydroxyl groups of the tyrosine triad.

Unfolding Kinetics. The unfolding of the mutant enzymes was monitored by measuring the fluorescence intensity upon the change of time at various urea concentrations. The unfolding curve was nicely fitted by one exponential function described in the eq 6. The unfolding rate of all the mutant proteins was fast relative to that of WT, suggesting that the tyrosine residues play arole in the structural integrity of KSI. When plots of RT ln k_U versus the urea concentration were made in the range where the proteins are unfolded more than 95% at equilibrium, straight lines were obtained (Figure 7). Thermodynamic parameters for free energy of unfolding for the wild-type and mutant enzymes are shown in Table 5. The kinetic data revealed that $\Delta G_U^{H_2O‡}$ is decreased by ca. 1.4, 3.4, and 1.7 kcal/mol for Y14S, Y30S, and Y55S, respectively. The decreases in $\Delta G_U^{H_2O‡}$ for the mutants might be due to the already exposed structure of the mutant resulting from the perturbation of α-helices in the native state, which might induce the decrease of the catalytic activities of the mutant enzymes. The mutational effect on stability for the transition state is also reflected in the $m_U^‡$ value. The ratio, $m_U^‡/m_U$, was reported to be the indication of the increase in solvent exposure of the transition state relative to the native state when normalized by the increase in solvent exposure between the native and denatured states (*32*). The ratio of $m_U^‡/m_U$ was 0.149 for WT, implying that the solvent accessibility of a transition state during the unfolding process is very similar to that of the native state, i.e., 14.9% of the buried hydrophobic surface in the native state is exposed at the transition state. The ratios for the mutant proteins were marginally decreased relative to that of WT.

Analyses of the Transition-State Interactions. The interactions mediated by three tyrosine residues during the unfolding process could be investigated utilizing a parameter Φ_U according to the method described previously (*33*). The large value of Φ_U implies that the target region is exposed to solvent in the transition state to the same extent as in the unfolded state, while the low value of Φ_U implies that the interaction energies in the transition states and folded states are very similar. There were only minor differences between the Φ_U value observed at 4 M urea and that obtained by the extrapolation to 0 M urea, indicating that there was no significant change of Φ_U values upon the change of urea concentration. The mutant proteins, Y14S, Y30S, and Y55S, gave the Φ_U values of 0.119, 0.248, and 0.179, respectively, indicating that the interactions mediated by three tyrosine residues in the native state are marginally weakened in the transition state. These values of Φ_U are consistent with those of the ratio, $m_U^‡/m_U$, during the unfolding process. Although the values of Φ_U and those of $m_U^‡/m_U$ for unfolding were marginally affected by the mutations, it seems that there is an inverse correlation with the loss of activities. Thus, these observations together with the decreases of $\Delta G_U^{H_2O‡}$ might suggest that the perturbation of the secondary structures in the native state affects the unfolding process of the mutant enzymes, resulting in the loss of the activities.

DISCUSSION

Our study was designed to address the contribution of the aromatic moieties in the active-site tyrosines of KSI to catalytic activity and stability. The significant decrease of $\Delta G_U^{H_2O}$ values for the serine mutants of the active-site tyrosines together with the crystal structure of Y55S and the far-UV CD spectra of the mutant proteins suggested that the hydrophobic packing mediated by three aromatic groups in the active-site tyrosine triad contributed significantly to conformational stability through maintaining the stable

Table 5: Changes in Free Energies of Native State ($\Delta\Delta G_U$) and Transition State ($\Delta\Delta G_U^‡$) for Unfolding upon Mutation of KSI[a]

enzyme	$\Delta G^‡_U{}^{H_2O}$[b] (kcal/mol)	$m^‡_U$[c] (kcal/mol·M)	$\Delta\Delta G_U$[d] (kcal/mol)	$\Delta\Delta G^‡_U$[e] (kcal/mol)	$\Delta\Delta G^‡_U{}^{[urea]4M}$[f] (kcal/mol)	$\Delta\Delta G^‡_U/\Delta\Delta G_U$ (in H_2O)	$\Delta\Delta G^‡_U{}^{[urea]4M}/\Delta\Delta G_U$ (at 4 M urea)	$m^‡_U/m_U$
WT	27.9	0.504						0.149
Y14S	26.5	0.437	11.9	1.4	1.1	0.119	0.093	0.149
Y30S	24.5	0.343	13.7	3.4	2.7	0.248	0.197	0.135
Y55S	26.2	0.408	9.5	1.7	1.3	0.179	0.137	0.119

[a] Measurements were carried out at 25 °C and pH 7.0. [b] $\Delta G^‡_U{}^{H_2O}$ was obtained from extrapolation of $\Delta G^‡_U$ to absence of urea where $\Delta G^‡_U$ was determined from the fit according to the equation, $k_U = (k_BT/h)\exp\{-\Delta G^‡_U/RT\}$. [c] $m^‡_U$ is the slope of the linear denaturation plot, $d\Delta G^‡_U/d[urea]$. [d] Values obtained from eq 5. [e] Values obtained from eq 9. [f] $\Delta\Delta G^‡_U{}^{[urea]4M}$ was determined by subtracting $\Delta G^‡_U$ at 4 M urea for each mutant from WT.

α-helices. The mutational effects on activity also revealed that the phenyl rings of Tyr14 and Tyr55 might play a role in efficient catalysis, while the mutational effect by Y30S was marginal. The Φ_U-value analysis suggests that the aromatic interactions of the tyrosine triad in the native state are maintained in the transition state.

It is very interesting that the 33-fold decrease of k_{cat} by the Y14S mutation is not very significant as compared with that by the Y14F mutation, for which k_{cat} is decreased by about 2000-fold. The Y14F mutation eliminates the hydroxyl group involved in the hydrogen bond critical to the stabilization of the intermediate in the catalysis of KSI, while the mutation did not affect significantly the structural integrity (*12*). On the other hand, the Y14S mutation retains the critical role of the hydroxyl group and changes significantly the secondary structure of the KSI protein as exhibited by the far-UV CD spectrum. Recently, we found that equilenin binds backward to the active site of the D38N/Y14F mutant (Choi et al., unpublished data). The substantial decrease in k_{cat} can be considered as a combined effect of the loss of the low barrier hydrogen bond and the nonproductive binding of the substrate. A much smaller decrease in k_{cat} by the Y14S mutation indicates that the substrate binds normally to the active site of this mutant. Thus, although the phenyl ring of Tyr14 is not critically essential for catalysis, it can affect indirectly the enzymatic function through maintaining the secondary structure. Tyr30 of *P. putida* KSI is replaced with Phe30 in *C. testosteroni* KSI. However, Tyr14 and Tyr55 are conserved in both KSIs. Therefore, the hydroxyl group of Tyr30 might not be critical for the catalytic activity of KSI since small decreases in k_{cat} were observed for both Y30S and Y30F (*12*). But the far-UV CD spectra in the equilibrium unfolding experiment of Y30S suggested that the presence of a bulky residue at this position is important not only for the protein stability but also for maintenance of the secondary structure of KSI. The effect of replacing Tyr55 with serine, a less hydrophobic and smaller residue, on catalysis could be explained by the structural changes of the enzyme as indicated by the crystal structure and the far-UV CD spectrum of Y55S. The previous study suggested that Tyr14 alone could not play the catalytic role efficiently without assistance by the hydrogen bond from either Tyr55 or Asp99 (*12*). The Y55S mutation gave rise to the disruption of the hydrogen bond between Tyr14 and Tyr55 as well as the H-bonded network, Tyr14···Wat504···Asp99. Thus, Tyr14 cannot function optimally without the assistance from both Tyr55 and Asp99. The structural perturbations at the active site could account for the large decrease of k_{cat} by about 51-fold for Y55S. In addition, the crystal structure of Y55S clearly showed that the phenyl ring of Tyr55 as a hydrophobe is important for the structural integrity of the α-helix to maintain the optimal active-site geometry even if Tyr55 does not seem to contribute directly to catalysis (*34*). Our results demonstrate that the substitutions of Tyr55 with serine could not provide a large apolar cleft to place the catalytic residues in the optimal position for efficient catalysis. Therefore, it can be proposed that the phenyl ring of Tyr55 is important in maintaining the structure of the active-site cavity for catalysis for the hydroxyl group of Tyr55 to stabilize the intermediate by forming the hydrogen bond with Tyr14 optimally and directionally.

Our recent analysis suggested that the folding of KSI could be driven mainly by the nonpolar active-site cavity formation (*35*). Furthermore, almost identical far-UV CD spectra for the mutants with tyrosine-to-phenylalanine replacement suggests that the internal packing rather than the hydrogen bonds contributes more significantly to the stabilization of the α-helices. The tyrosine triad is shielded from solvent, which is thought to be one of the main sources of stabilization energy. Crystallographic analysis has shown that side chains in the interior of protein are very closely packed, occupying almost all the available interior space (*8*). Little differences in the geometry of the phenyl rings between WT and a tyrosine triple mutant, Y14F/Y30F/Y55F, in which all three tyrosine residues were replaced with phenylalanine residues (*18*), suggests that the aromatic rings of tyrosine residues are more important for the orientation of the ring geometry rather than the hydrogen bonds. Our results demonstrate that the phenyl rings of the tyrosine residues are important for structural stability since they maintain internal packing in the interior of KSI to stabilize the α-helices.

The H-bonded network is prevalent in enzyme systems. Particularly, tyrosine residues are often found to form the H-bonded network since they seem to satisfy the internal packing and ionic interaction leading to the optimization of the conformational stability as well as enzymatic function. The roles of the H-bonded network mediated by the hydroxyl groups of tyrosine residues in both protein structure and function have been previously studied (*12*, *36*−*38*). Tyr52 and Tyr73 forming a H-bonded network in PLA_2 were found to play a structural role in efficient catalysis (*36*). In case of human manganese superoxide dismutase, disruption of the H-bonded network at the active site decreased k_{cat} by 10- to 40-fold and the melting temperature by 10−16 °C (*38*). However, a few studies on the roles of phenyl rings in the H-bonded network have been reported. The active site of PLA_2 contains such conserved residues as Tyr52 and Tyr73. Substitution of either tyrosine residue with aliphatic amino acids decreased both activity and stability more significantly than that with phenylalanine (*39*). Studies on ribonuclease A showed that the replacement of a catalytic residue, Tyr97, with a phenylalanine, alanine, or glycine residue diminished the catalytic activity by 3-, 250-, or 500-fold, respectively (*40*). The free energies of Y97F, Y97A, and Y97G decreased by 3.5, 12.0, and 11.7 kcal/mol, respectively, relative to that of WT, suggesting that the aromatic moieties contribute to stability as well as catalysis.

The H-bonded network of the tyrosine residues seems to be maintained in the transition state for unfolding as reflected in the value of Φ_U, implying that the interactions mediated by the tyrosine residues are resistant to external perturbation. In addition, the internal packing by the phenyl ring structures rather than the hydrogen bonds network of tyrosine residues might be more significant for the favorable folding of KSI since KSI could be refolded normally upon the triple tyrosine mutation, Y14F/Y30F/Y55F (*18*). Given that approximately 80−90% interactions mediated by the aromatic moieties of Tyr14 and Tyr55 are present in the transition state during the unfolding process, one can expect that the tyrosine residues can interact significantly in the transition state. These results suggest that the three tyrosine residues located at the core of the active site might interact with one another in the transition state for unfolding.

In conclusion, the mutational studies on the roles of the aromatic groups of the active-site tyrosine residues demonstrate that the phenyl rings contribute to enzymatic function as well as the conformational stability by maintaining the structural integrity of the α-helices. Further analysis should be carried out to identify the origin of decrease for the content of α-helix in the mutant enzymes on the basis of three-dimensional structures of the mutant enzymes. These studies will contribute to the better understanding of the roles of the internal aromatic residues in the enzymatic systems.

ACKNOWLEDGMENTS

This paper is dedicated to Prof. Sang Chul Shim on the occasion of his retirement.

REFERENCES

1. Batzold, F. H., Benson, A. M., Covey, D. F., Robinson, C. H., and Talalay, P. (1976) *Adv. Enz. Regul. 14*, 243−267.
2. Radzicka. A., and Wolfender, R. (1995) *Science 267*, 90−93.
3. Xue, L., Kuliopulos, A., Milvan, A. S., and Talalay, P. (1991) *Biochemistry 30*, 4991−4997.
4. Xue, L., Talalay, P., and Milvan, A. S. (1991) *Biochemistry 30*, 10858−10865.
5. Hawkinson, D. C., Eames, T. C., and Pollack, R. M. (1991) *Biochemistry 30*, 10849−10858.
6. Hawkinson, D. C., Pollack, R. M., and Ambulos, N. P., Jr. (1994) *Biochemistry 33*, 12172−12183.
7. Kim, S. W., Cha, S.-S., Cho, H.-S., Kim, J.-S., Ha, N.-C., Cho, M.-J., Joo, S., Kim, K.-K., Choi, K. Y., and Oh, B.-H. (1997) *Biochemistry 36*, 14030−14036.
8. Cho, H.-S., Choi, G., Choi, K. Y., and Oh, B.-H. (1998) *Biochemistry 37*, 14030−14036.
9. Wu, Z. R., Ebrahimian, S., Zawrotny, M. E., Thornburg, L. D., Perez-Alvarado, G. C., Brothers, P., Pollack, R. M., and Summers, M. F. (1997) *Science 276*, 415−418.
10. Massiah, M. A., Abeygunawardana, C., Gittis, A. G., and Mildvan, A. S. (1998) *Biochemistry 37*, 14701−14712.
11. Cho, H.-S., Ha, N. C., Choi, G., Kim, H. J., Lee, D., OH, K. S., Kim, K. S., Lee, W., Choi, K. Y., and Oh, B.-H. (1999) *J. Biol. Chem. 274*, 32863−32868.
12. Kim, D.-H., Jang, D. S., Nam, G. H., Choi, G., Kim, J.-S., Ha, N.-C., Kim, M.-S., Oh, B.-H., and Choi, K. Y. (2000) *Biochemistry 39*, 4581−4589.
13. Burley, S. K., and Petsko, G. A. (1985) *Science 229*, 23−28.
14. Serrano, L., Bycroft, M., and Fersht, A. R. (1991) *J. Mol. Biol. 218*, 465−475.
15. Sekharudu, C., Ramakrishnan, B., Huang, B., Jiang, R. T., Dupureur C. M., Tsai, M. D., and Sundaralingam, M. (1992) *Protein Sci. 12*, 1585−1594.
16. Anderson, D. E., Hurley, J. H., Nicholson, H., Baase, W. A., and Matthew, B. W. (1993) *Protein Sci. 2*, 1285−1290.
17. Bromme, D., Bonneau, P. R., Purisima, E., Lachance, P., Hajnik, S., Thomas, D. Y., and Storer, A. C. (1996) *Biochemistry 13*, 3970−3979.
18. Choi, G., Ha, N.-C., Kim, M.-S., Hong, B.-H., Oh, B,-H.; Choi, K. Y. (2001) *Biochemistry, 40*, 6828−6835.
19. Copeland, R. A. (1993) *Methods of Protein Analysis*, Chapman and Hall, New York, NY.
20. Kunkel, T. A. (1985) *Proc. Natl. Acad. Sci. U.S.A. 82*, 488−492.
21. Kim, S. W., and Choi, K. Y. (1995) *J. Bacteriol. 177*, 2602−2605.
22. Kim, S. W., Kim, C. Y., Benisek, W. F., and Choi, K. Y. (1994) *J. Bacteriol. 176*, 6672−6676.
23. Otwinowski, Z. (1993) in *Proceedings of the CCP4 Study Weekend* (Sawyer, L., et al., Eds.), pp 56−62, SERC Daresbury Laboratory, Warrington, U.K.
24. Mok, Y.-K., Gay, G. D., Butler, P. J., and Bycroft, M. (1996) *Protein Sci. 5*, 310−319.
25. Yun, S., Jang, D. S., Kim, D.-H., Choi, K. Y., and Lee, H. C. (2001) *Biochemistry 40*, 3967−3973.
26. Zhao Q., Li Y. K., Mildvan A. S., and Talalay P. (1995) *Biochemistry 34*, 6562−6572.
27. Zhao Q., Abeygunawardana C., and Mildvan A. S. (1996) *Biochemistry 35*, 1525−1532.
28. McRee, D. E. (1993) *Practical Protein Crystallography*, pp 223−226, Academic Press, San Diego, U.S.A.
29. Luzzati, P. V. (1952) *Acta Crystallogr. 5*, 802−810.
30. Kim, D.-H., Nam, G. H., Jang, D. S., Choi, G., Joo, S., Kim, J.-S., Oh, B.-H., and Choi, K. Y. (1999) *Biochemistry 38*, 13810−13819.
31. Kraulis, P. J. (1991) *J. Appl. Crystallogr. 24*, 946−950.
32. Tanford, C. (1970) *Adv. Protein. Chem. 24*, 1−95.
33. Matouschek, A., Kellis, J., Serrano, L., and Fersht, A. R. (1989) *Nature 340*, 122−126.
34. Kuliopulos, A., Mildvan, A. S., Shortle D., and Talalay, P. (1989) *Biochemistry 28*, 149−159.
35. Kim, D.-H., Nam, G. H., Jang, D. S., Yun, S., Choi, G., Lee, H. C., and Choi, K. Y. (2001) *Protein Sci. 10*, 741−752.
36. Kuipers, O. P., Franken, P. A., Hendriks, R., Verheij, H. M., and Haas, G. (1990) *Protein Eng. 4*, 199−204.
37. Stickle, D. F., Presta, L. G., Dill, K. A., and Rose, G. D. (1992) *J. Mol. Biol. 226*, 1143−1159.
38. Ramilo, C. A., Leveque. V., Guan, Y., Lepock, J. R., Tainer, J. A., Nick, H. S., and Silverman, D. N. (1999) *J. Biol. Chem. 274*, 27711−27716.
39. Dupureur, C. M., Yu, B. Z., Jain, M. K., Noel, J. P., Deng, T., Li, Y., Byeon, I. J., and Tsai, M. D. (1992) *Biochemistry 28*, 6402−6413.
40. Eberhardt, E. S., Wittmayer, P. K., Templer, B. M., and Raines, R. T. (1996) *Protein Sci. 8*, 1697−1703.

BI015547K